Supporting Information for "The internal structure and dynamics of Jupiter unveiled by a high-resolution magnetic field and secular variation model"

S. Sharan[1], B. Langlais[1], H. Amit[1], E. Thébault[2], M. Pinceloup[1], and O.

Verhoeven[1]

[1]Laboratoire de Planétologie et Géosciences, CNRS UMR 6112, Nantes Université, Université d'Angers, Le Mans Université,

Nantes, France

[2]Laboratoire Magma et Volcans, Université Clermont Auvergne, UMR 6524, CNRS, IRD, OPGC, Clermont-Ferrand, France

Contents of this file

Text S1. Synthetic simulation

––––––––

Corresponding authors: S. Sharan, Laboratoire de Planétologie et Géosciences, CNRS UMR

6112, Nantes Université, Nantes, France (shivangi.sharan@univ-nantes.fr)

Corresponding authors: B. Langlais, Laboratoire de Planétologie et Géosciences, CNRS UMR

6112, Nantes Université, Nantes, France (benoit.langlais@univ-nantes.fr)

May 25, 2022, 7:56am

The internal Jovian magnetic field and its temporal rate of change (secular variation, SV) is expanded in terms of Spherical Harmonics (SH). Above the magnetic sources, the magnetic field $\mathbf{B}$ derives from the expression of a magnetic scalar potential V by $\mathbf{B} = -\nabla V$ and where in spherical coordinates it is approximated by the finite series

$$
\begin{aligned}
V(r, \theta, \phi, t) \;=\; & R_J \sum_{n=1}^{n_i^{max}} \sum_{m=0}^{n} \left\{ \left(\frac{R_J}{r} \right)^{n+1} (g_n^m(t) \cos m\phi + h_n^m(t) \sin m\phi) P_n^m(\cos\theta) \right\} \\
& + R_J \sum_{n=1}^{n_e^{max}} \sum_{m=0}^{n} \left\{ \left(\frac{r}{R_J} \right)^{n} (q_n^m(t) \cos m\phi + s_n^m(t) \sin m\phi) P_n^m(\cos\theta) \right\}
\end{aligned} \tag{1}
$$

where r denotes the radial distance from the center of Jupiter, R_J is Jupiter's equatorial radius equal to 71,492 km, θ the co-latitude, and ϕ the longitude. The functions $P_n^m(\cos\theta)$ are the Schmidt quasi-normalized associated Legendre functions of degree n and order m. The Gauss coefficients $g_n^m(t)$, $h_n^m(t)$ are the time-varying parameters to be estimated by inversion of the measurements conventionally given in the units of nano-Tesla (nT). The mathematical series in Eq.(1) is truncated to n_i^{max} and n_e^{max}, which are the maximum degrees for the internal and external field coefficients.

The three vector components of Jupiter's magnetic field in the radial, southward and eastward horizontal directions (B_r, B_θ and B_ϕ) are calculated from the negative gradient of Eq.(1) in the spherical coordinate system

$$
B_r = -\frac{\partial V}{\partial r}, \quad B_\theta = -\frac{1}{r}\frac{\partial V}{\partial \theta}, \quad B_\phi = -\frac{1}{r\sin\theta}\frac{\partial V}{\partial \phi}. \tag{2}
$$

In order to test the data distribution and its adequacy with model determination, we compute a set of synthetic vector magnetic field predictions at the actual Juno locations

May 25, 2022, 7:56am

and epochs using the CHAOS-7.8 Earth's magnetic field model (Finlay et al., 2020). This time-dependent model is based on magnetic field observations collected by the low-Earth orbiting satellites between years 1999 and 2021. It is expanded to SH degree $n_i^{max} = 20$ for the time varying internal field with order 6 B-splines (de Boor, 2001) with a 6-month knot separation. The synthetic data we build therefore contains a significant amount of rapid secular variation, secular acceleration, and contributions of higher time derivatives, including some geomagnetic jerks or core pulses, which are sudden changes in the second time derivative of the Earth's magnetic field (e.g., Aubert & Finlay, 2019).

Before predicting the field over the four years of available Juno data, we note that the strength and shape of Earth's and Jupiter's magnetic fields are different. Figure S4 shows the power spectra of Earth's main field CHAOS model, its secular variation, and the power spectrum of Jupiter's magnetic field model derived by Connerney et al. (2022), both at the reference radius of each planet.

In a first step towards building a realistic synthetic data set, we estimate by standard least-squares the power law of Jupiter's magnetic field model. For the CHAOS model, we estimate two power laws in order to account for the different internal field sources contributing to the model. Indeed, a distinct change of slope occurs around SH degree 13 that indicates that the field from the core dominates from SH degree 1 to 13, while the field from the crust dominates from SH degree 15 (Langel & Estes, 1982). For each part of the power spectrum we use the power law difference with Jupiter's model to rescale the CHAOS internal field model to SH degree 20. In addition, we impose that the power spectrum of the rescaled secular variation keeps the same slope as the original CHAOS

model. Without this precaution, the synthetic secular variation power spectrum diverges at the dynamo radius of Jupiter. The power spectra of the rescaled CHAOS main field model, following now the general trend of the model by Connerney et al. (2022), and its secular variation are displayed in Figure S4.

The rescaling of the CHAOS model allows us to incorporate the a priori information provided with Juno data. In the database, each measurement is given with a precision index corresponding to the magnetometer operating range and an instrumental noise less than 1 nT. The uncertainties are defined for six different operating ranges and vary with the strength of the ambient magnetic field (Connerney et al., 2017). Each synthetic observation we build is therefore associated with a weight (with a minimum weight of 1 nT) and we further add a Gaussian random noise of 25 nT to each vector measurement. This Gaussian noise is the upper bound of the instrument error of Juno measurements.

We then set up the parameterization of the inverse problem. The internal static field is derived up to SH degree $n_i^{max} = 20$ and a static external field to SH degree 2. The maximum resolution of the internal time variation of the model is imposed by the time difference and the spatial coverage between Juno's polar orbits. We choose to parameterize the time variation with splines of order 2 with a knot spacing of 2 years and for SH degrees 1 to 10 only. The examination of the covariance matrix indicates that we are not dealing with an ill-conditioned inverse problem that would require an explicit regularization. The 608 coefficients are then estimated by weighted least-squares and the inversion is performed with a singular value decomposition (SVD) algorithm, thus offering

the possibility at a later stage to solve the problem with the generalized truncated SVD technique.

The results of the synthetic inversion is assessed in the spatial and spectral domains using several criteria (see Alken et al. (2021) for a list of possible criteria). We show in Figure S5 the power spectrum of the estimated model with the power spectrum of the input rescaled CHAOS model for the main field and its secular variation. These are accompanied with the results of the spherical harmonic correlation analysis. Both power spectra for the main field agree in strength and correlate better than 0.99 over the full degree range. For the SV the correlation is better than 0.75. However, we observe an increase in the estimated power spectrum starting from SH degree 8. This overestimated energy compared to the rescaled CHAOS benchmark model is the sign of power leakage from the time-varying structures that are not accounted for in the estimated model. Figure S6 shows the input and output radial field and its difference at $\mathbf{R}_{sf}$ (0.83 times Jupiter's radius) to SH degree 20 for the static part and to SH degree 8 for the SV part. We observe no significant residuals for the static field while the SV residuals follow the SV structures. The residuals are one order of magnitude smaller than the input SV model indicating the presence of a small power leakage that is amplified at the dynamo radius.

Text S2. Dynamo Radius Estimate

For Earth, the geomagnetic field spectrum (Lowes, 1966) can be steadily interpreted in terms of magnetic source location. There is an apparent slope break near degrees 13-14 that distinguishes between the energy from the core and crustal field components, respectively. Ignoring the dipole term, the spectrum becomes almost flat when downward

extrapolated to the CMB for the core part, while it shows an almost null slope at the surface for higher degrees. This property has been observed for a long time (Lowes, 1974) and has been suggested to provide a crude estimate of the core radius on other planets where seismological measurements are not available.

This crude estimate can be refined by using alternative expressions to the power spectrum. McLeod (1996) defined an expression using magnetic monopoles to estimate core radius. Langlais, Amit, Larnier, Thébault, and Mocquet (2014) defined two additional expressions, first using the non-zonal terms ($m \neq 0$) and the second using the quadrupole terms ($n + m$ even). These two sub-families show flat spectra independent of degree n at a radius r, interpreted as the CMB for Earth (Figure S7). The non-zonal spectrum has a null slope immediately above the dynamo area. This is expected because the geomagnetic field is axisymmetric on the long term, and the non-axisymmetric part is thought to be random. The flatness of the quadrupole family spectrum is explained by the dominance of rotational effects in the dynamo process. They can be defined as

$$\mathcal{R}_n^{nz}(r) = (n+1)\left(\frac{a}{r}\right)^{(2n+4)} \sum_{m=1}^{n} [(g_n^m)^2 + (h_n^m)^2] \tag{3}$$

$$\mathcal{R}_n^{qf}(r) = (n+1)\left(\frac{a}{r}\right)^{(2n+4)} \sum_{m=0,\ n+m\ even}^{n} [(g_n^m)^2 + (h_n^m)^2] \tag{4}$$

where a is the reference radius, equal to the planet's radius.

The $\mathcal{R}_n^{nz}$ and $\mathcal{R}_n^{qf}$ provide a close estimate of the core radius as was verified using four different geomagnetic models (Langlais et al., 2014). For CHAOS-4 field model at epoch 2005 and $n = 13$, the estimated core radius R_{nz} estimated from Eq.(3) is 3,486.6 km and the R_{qf} estimated from Eq.(4) is 3,496.7 km, which are similar to the accepted

seismic value of 3,481.7 km. The maximum likelihood value using the approach of Lowes (1974) gives R_{lowes}=3,294.5 km and the one using the approach of McLeod (1996) provides R_{mcleod}=3,586.5 km, both deviating significantly from the accepted seismic value. The core (or dynamo) radii for other planets were also estimated. Using the JSV model of Ridley and Holme (2016) for Jupiter up to $n = 5$, Langlais et al. (2014) provided the values 0.86 and 0.87 R_J for R_{nz} and R_{qf} respectively. For our model, we estimate the dynamo radius for both the non-zonal and quadrupole families (Figure S8) by varying the truncation degree between 10 and 20, and observe that the slope is the most flat at $n = 16$. The radius starts to increase beyond it. The non-zonal spectrum gives a value of 0.831 R_J with a standard deviation of 0.021 R_J, while the quadrupole family spectrum returns 0.829 R_J with a standard deviation of 0.024 R_J. Both independent estimates therefore fall within each other's error bars. The mean of the radii estimated using $n_i^{max} = 16$ corresponds to 0.830±0.022 R_J.

References

Alken, P., Thébault, E., Beggan, C. D., Aubert, J., Baerenzung, J., Brown, W. J., . . . Wardinski, I. (2021). Evaluation of candidate models for the 13th generation international geomagnetic reference field. *Earth, Planets and Space*, *73*(1), 48. Retrieved from `https://doi.org/10.1186/s40623-020-01281-4`   doi: 10.1186/s40623-020-01281-4

Aubert, J., & Finlay, C. C. (2019). Geomagnetic jerks and rapid hydromagnetic waves focusing at earth's core surface. *Nature Geoscience*, *12*(5), 393–398. Retrieved from `https://doi.org/10.1038/s41561-019-0355-1` doi: 10.1038/s41561-019-0355-1

Connerney, J. E. P., Benn, M., Bjarno, J. B., Denver, T., Espley, J., Jorgensen, J. L., . . . Smith, E. J. (2017). The juno magnetic field investigation. *Space Science Reviews*, *213*(1), 39–138. Retrieved from `https://doi.org/10.1007/s11214-017-0334-z` doi: 10.1007/s11214-017-0334-z

Connerney, J. E. P., Timmins, S., Oliversen, R. J., Espley, J. R., Joergensen, J. L., Kotsiaros, S., . . . Levin, S. M. (2022). A new model of jupiter's magnetic field at the completion of juno's prime mission. *Journal of Geophysical Research: Planets*, *127*(2), e2021JE007055. Retrieved from `https://agupubs.onlinelibrary.wiley.com/doi/abs/10.1029/2021JE007055` (e2021JE007055 2021JE007055) doi: `https://doi.org/10.1029/2021JE007055`

de Boor, C. (2001). Calculation of the smoothing spline with weighted roughness measure. *Mathematical Models and Methods in Applied Sciences*, *11*(01), 33-41. Retrieved from `https://doi.org/10.1142/S0218202501000726` doi: 10.1142/S0218202501000726

Finlay, C. C., Kloss, C., Olsen, N., Hammer, M. D., Tøffner-Clausen, L., Grayver, A., & Kuvshinov, A. (2020). The chaos-7 geomagnetic field model and observed changes in the south atlantic anomaly. *Earth, Planets and Space*, *72*(1), 156. Retrieved from `https://doi.org/10.1186/s40623-020-01252-9` doi: 10.1186/s40623-020-01252 -9

Langel, R. A., & Estes, R. H. (1982). A geomagnetic field spectrum. *Geophysical Research Letters*, *9*(4), 250-253. Retrieved from `https://agupubs.onlinelibrary.wiley.com/doi/abs/10.1029/GL009i004p00250` doi: `https://doi.org/10.1029/`

GL009i004p00250

Langlais, B., Amit, H., Larnier, H., Thébault, E., & Mocquet, A. (2014). A new model for the (geo)magnetic power spectrum, with application to planetary dynamo radii. *Earth and Planetary Science Letters*, *401*, 347-358. Retrieved from `https://www.sciencedirect.com/science/article/pii/S0012821X14003070` doi: https://doi.org/10.1016/j.epsl.2014.05.013

Lowes, F. J. (1966). Mean-square values on sphere of spherical harmonic vector fields. *Journal of Geophysical Research (1896-1977)*, *71*(8), 2179-2179. Retrieved from `https://agupubs.onlinelibrary.wiley.com/doi/abs/10.1029/JZ071i008p02179` doi: https://doi.org/10.1029/JZ071i008p02179

Lowes, F. J. (1974, 03). Spatial power spectrum of the main geomagnetic field, and extrapolation to the core. *Geophysical Journal International*, *36*(3), 717-730. Retrieved from `https://doi.org/10.1111/j.1365-246X.1974.tb00622.x` doi: 10.1111/j.1365-246X.1974.tb00622.x

McLeod, M. G. (1996). Spatial and temporal power spectra of the geomagnetic field. *Journal of Geophysical Research: Solid Earth*, *101*(B2), 2745-2763. Retrieved from `https://agupubs.onlinelibrary.wiley.com/doi/abs/10.1029/95JB03042` doi: https://doi.org/10.1029/95JB03042

Ridley, V. A., & Holme, R. (2016). Modeling the jovian magnetic field and its secular variation using all available magnetic field observations. *Journal of Geophysical Research: Planets*, *121*(3), 309-337. Retrieved from `https://agupubs.onlinelibrary.wiley.com/doi/abs/10.1002/2015JE004951` doi: https://doi
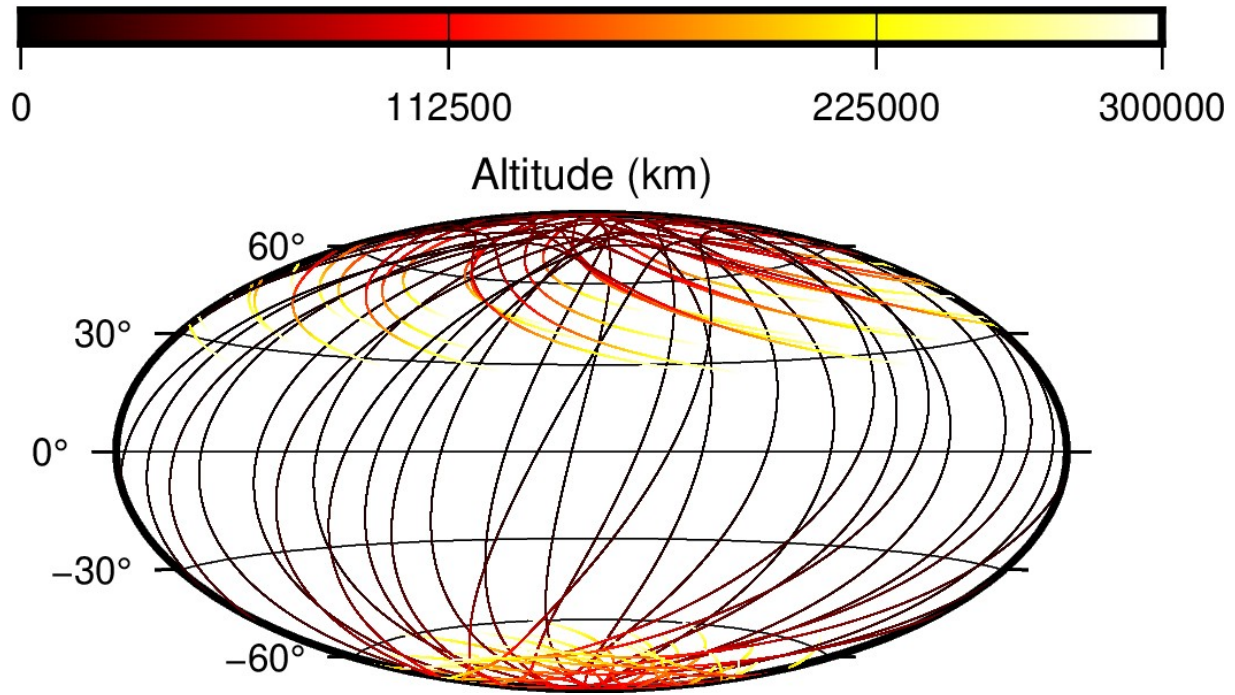
Figure S1. The data locations of Juno satellite below 300,000 km for the first 28 (without orbit 2 and 19) perijoves. The colour scale represents the altitude above the mean radius. The map is centered at 180° longitude.

May 25, 2022, 7:56am
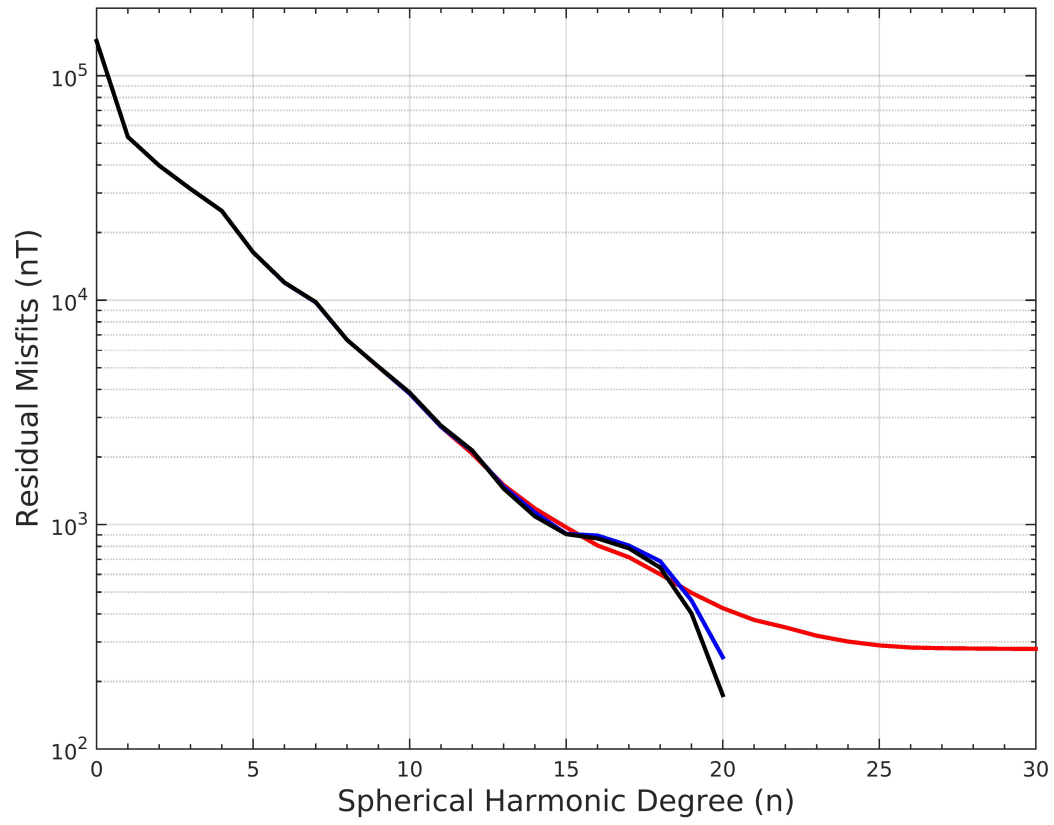
Figure S2.   The residual misfits plotted as a function of the SH degree for the model

by Connerney et al. (2022) (red), a model without SV (blue) and our model (black).
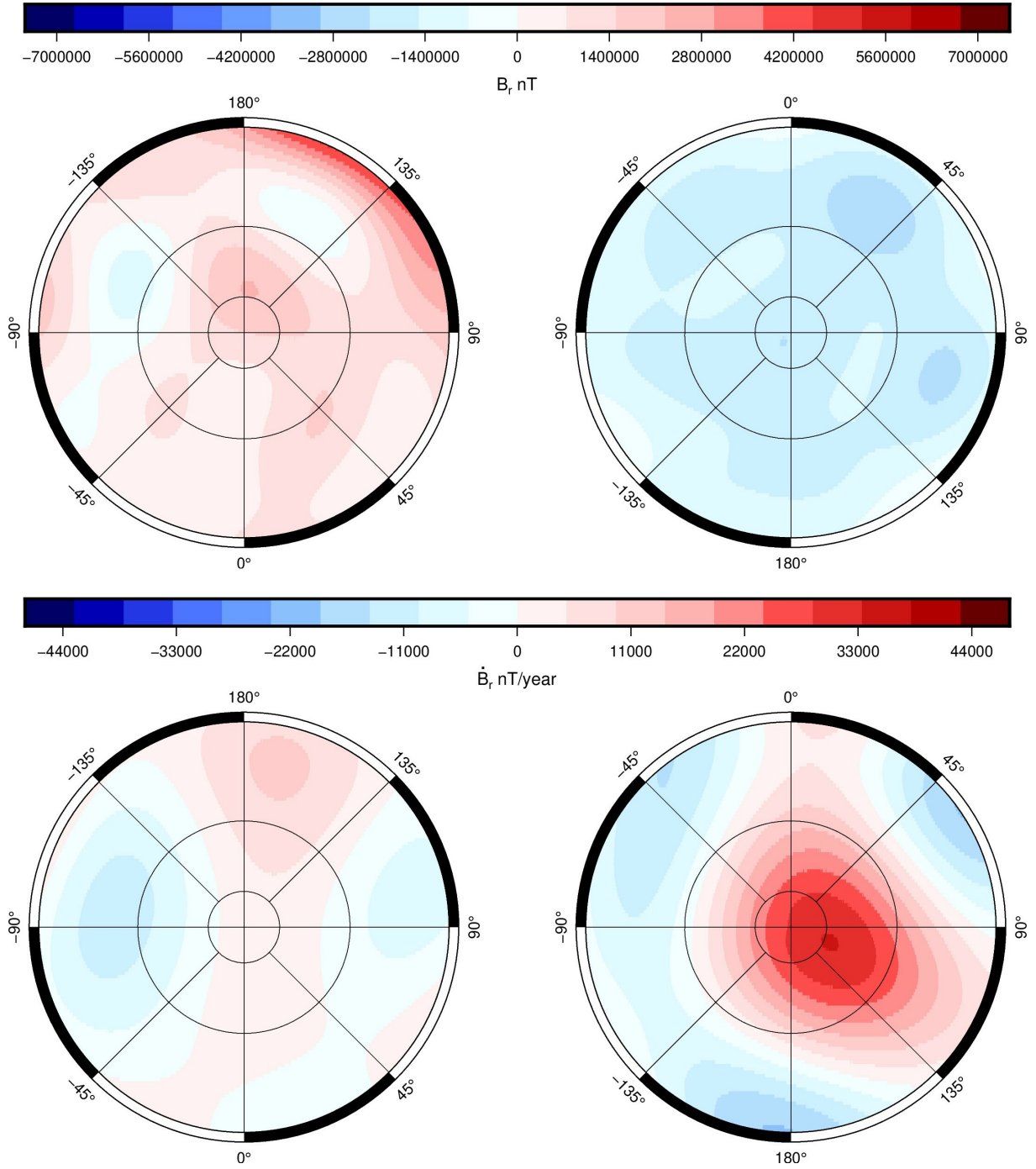
Figure S3. The (top) radial field and (bottom) radial secular variation at the estimated dynamo radius $\mathbf{R}_{sf}$ for the (left) North Pole and (right) South Pole. The inner to outer circles represent latitudes 85°, 75° and 60° respectively.

May 25, 2022, 7:56am
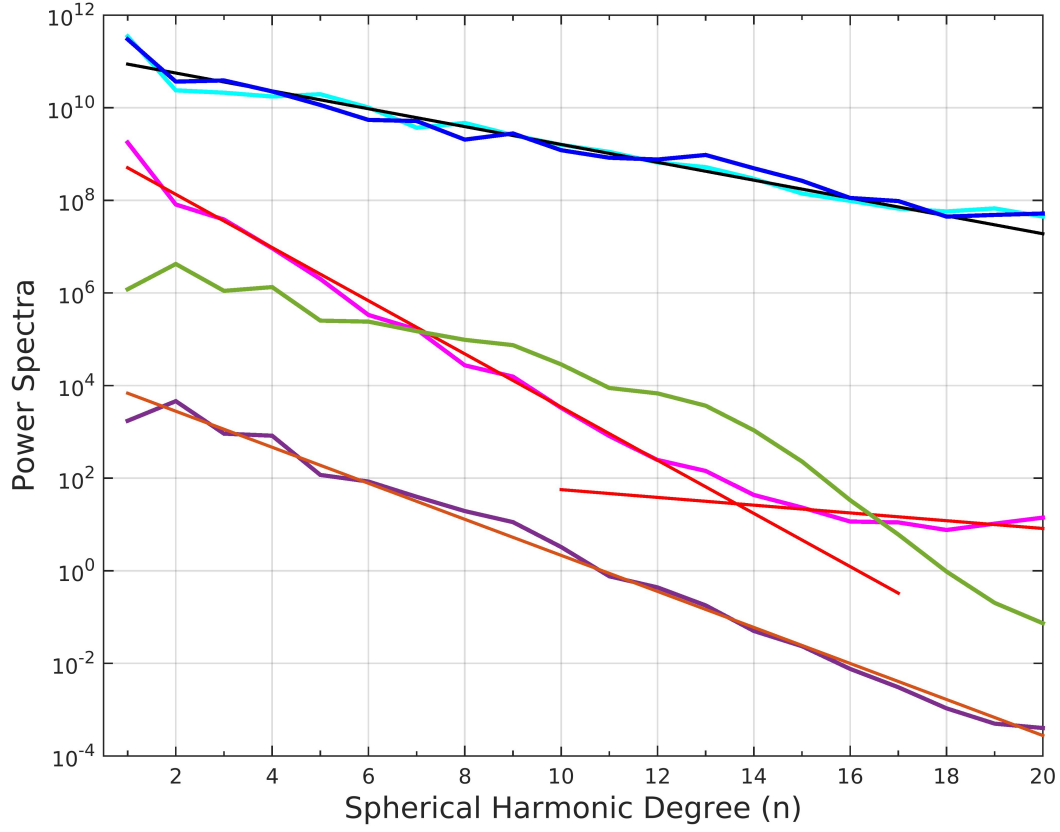
Figure S4. (a) The initial power spectrum of the CHAOS-7.8 main field model (magenta), its SV (purple) and the spectrum of Connerney et al. (2022) main field (cyan). The red, orange and black straight lines are the power law rules estimated by least-squares fits for these models respectively. The power laws for the CHAOS main field model (red lines) are different from degrees 1 to 13 and from degrees 14 to 20 (Text S1 for details). The new rescaled CHAOS-7.8 main field and SV models are shown in blue and green respectively. The units for main field are nT^2 and $(nT/year)^2$ for SV spectra.
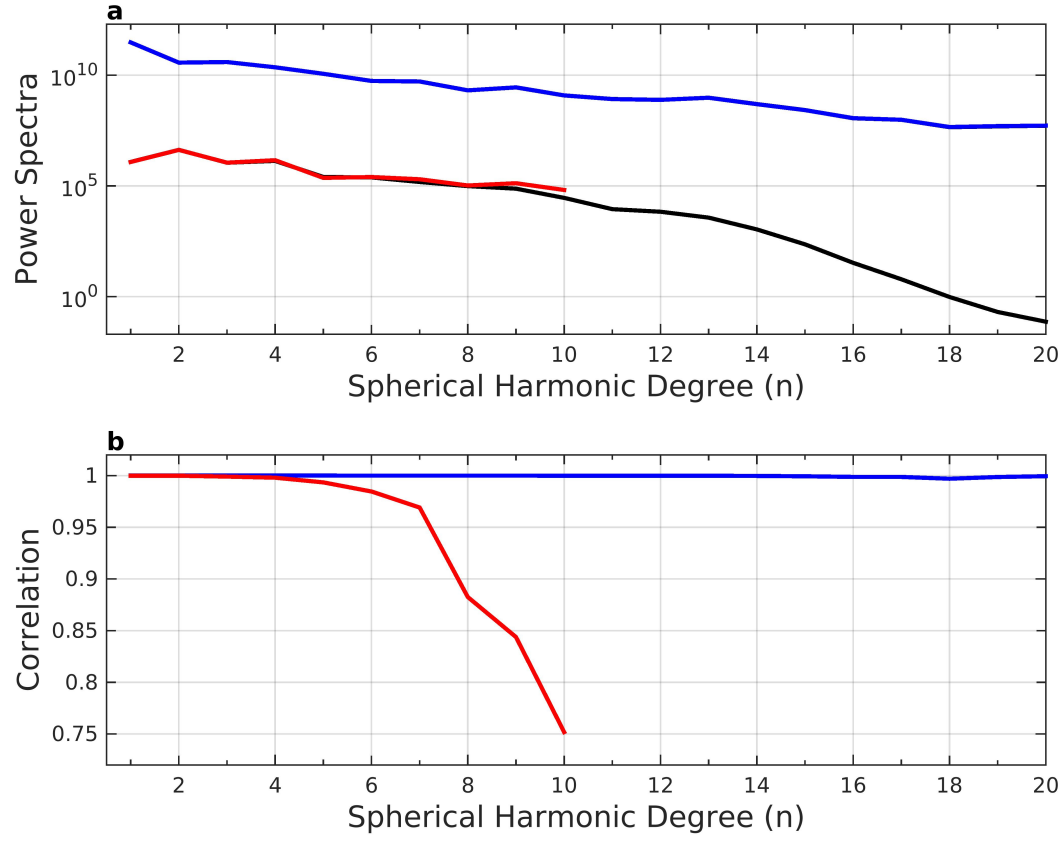
Figure S5. (**a**) The power spectrum of the main field (in blue with units of nT^2) and secular variation (in red with units of $(nT/year)^2$) of the estimated and input (black) magnetic field models at the Jovian surface. (**b**) The spherical harmonic correlation between the estimated and the input models for the main field (blue) and the SV (red).
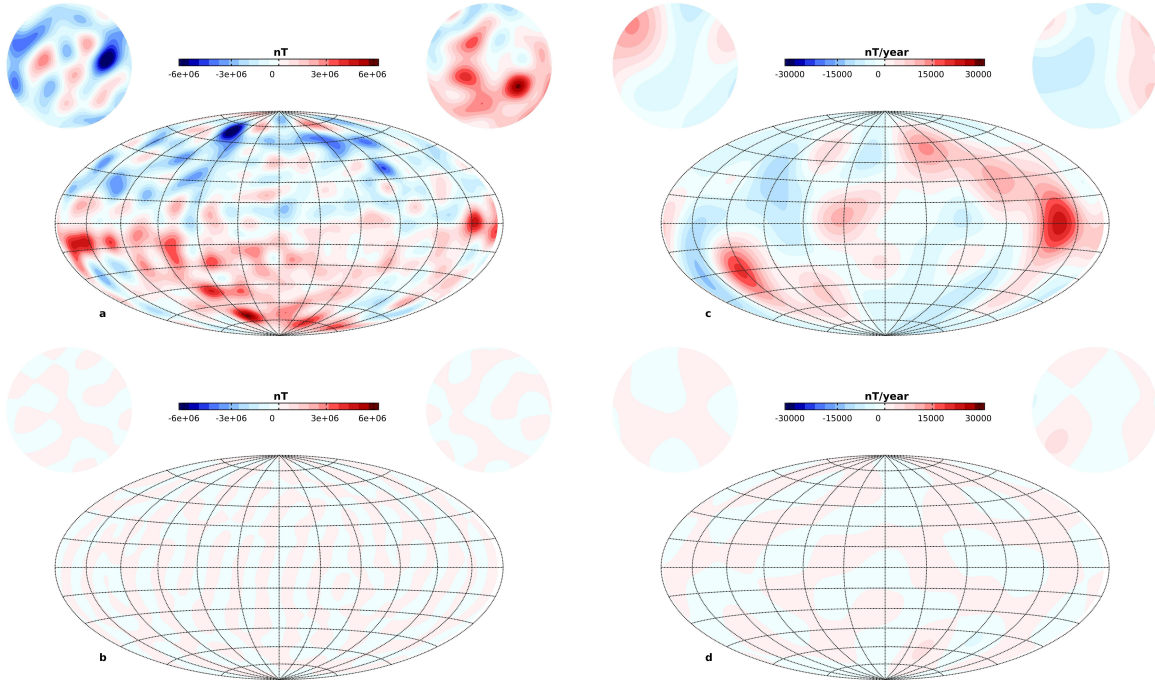
Figure S6. The (**a**) radial field of the estimated model and the (**b**) difference of the radial field between the input and estimated model in the synthetic analysis. The (**c**) radial SV of the estimated model and the (**d**) difference of the radial SV between the input and estimated model in the synthetic analysis. The maps are centered at 180° longitude and plotted at $\mathbf{R}_{sf}$.
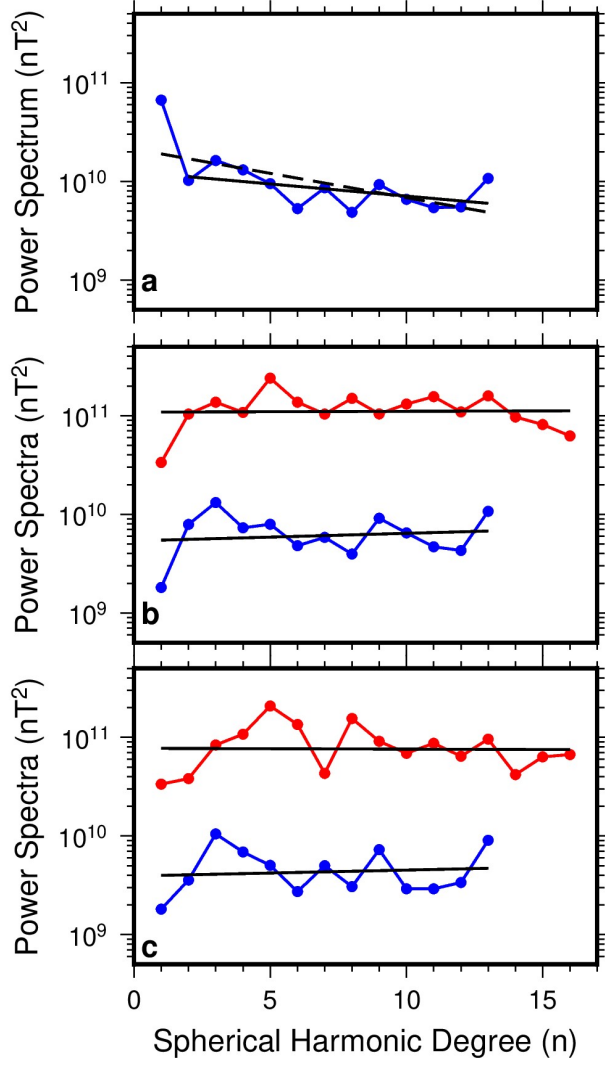
Figure S7. (a) Geomagnetic power spectrum of CHAOS-7.8 model at the CMB with linear regression from n=1-13 (black dashed line, slope = -0.0493) and 2-13 (black line, slope = -0.0245). (b) The non-zonal spectra with linear regression (black line) for the geomagnetic model (blue, slope = 0.0077) at CMB and for our model (red, slope = 0.0008) at the estimated dynamo radius $\mathbf{R}_{sf}$. (c) The quadrupole family spectra with linear regression (black line) for the geomagnetic field (blue, slope = 0.0060) at CMB and for our model (red, slope = 0.0008) at the estimated dynamo radius $\mathbf{R}_{sf}$.

May 25, 2022, 7:56am
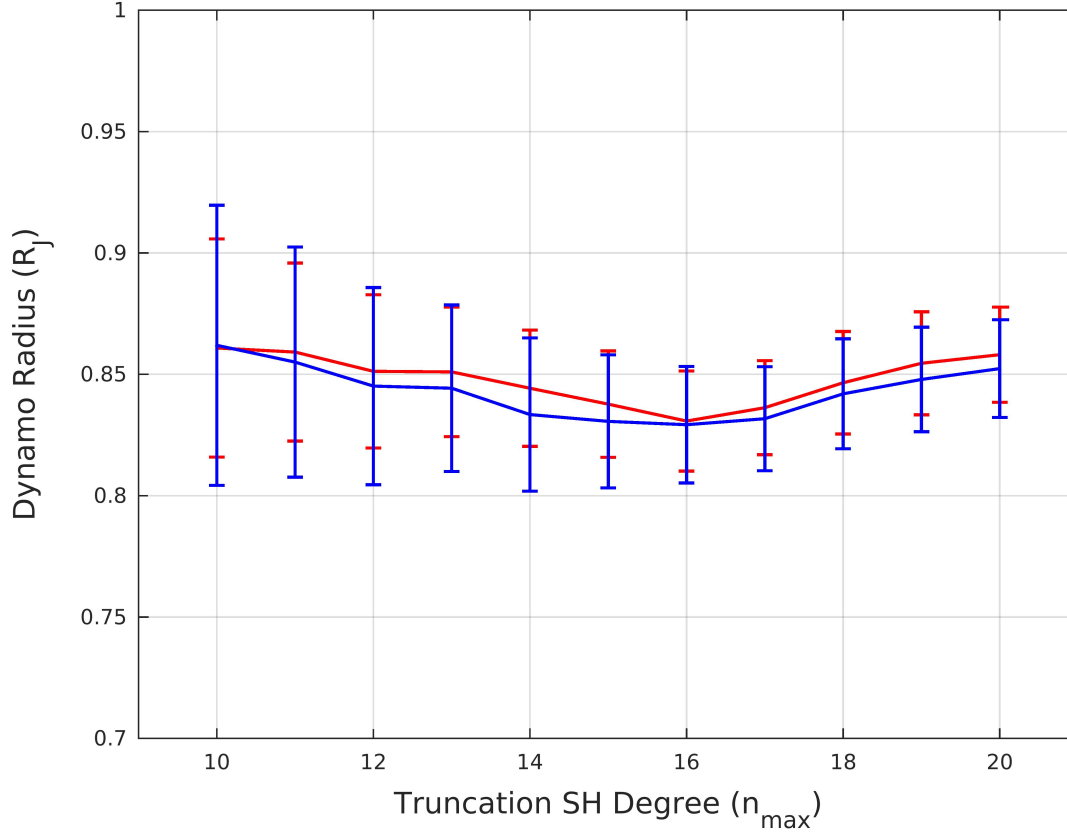
Figure S8. The dynamo radius estimates with the error bounds calculated using the non-zonal (red) and quadrupole (blue) terms at different truncation degrees using the estimated Jovian magnetic field model.

Table S1. Inversion misfits (in nT) for models without and with secular variation ($n_i^{max} = 20$ and 8 for the main field and SV respectively).

	B_r	B_θ	B_ϕ	$\mathbf{B}$
model without SV	286	264	357	305
model with SV	176	203	176	186

May 25, 2022, 7:56am